Solid State Communications, Vol. 25, pp. 93–99, 1978. Pergamon Press. Printed in Great Britain

ANGLE RESOLVED PHOTOEMISSION FROM ADSORBATES: THEORETICAL CONSIDERATIONS OF POLARIZATION EFFECTS AND SYMMETRY*

M. Scheffler and K. Kambe

Fritz-Haber-Institut der Max-Planck-Gesellschaft Faradayweg 4-6, 1000 Berlin 33, West Germany

and

F. Forstmann

Freie Universität Berlin, Inst. für Theor. Physik Arnimallee 3, 1000 Berlin 33, West Germany

(*Received* 10 *June* 1977 *by M. Cardona*)

Angular distributions of photoemission from chemisorption induced states and LEED spectra are calculated for the $p(2 \times 2)$ and the $c(2 \times 2)$ oxygen superstructure on the (001) surface of nickel. The obtained dependence of the photoemission intensity on the polar angle, on the azimuth angle of emission and on the direction of the light beam is discussed using mainly symmetry arguments (selection rules). This kind of analysis is shown to be useful for identifying the orbital symmetry or the symmetry of the adsorbate position without carrying out complicated calculations.

1. INTRODUCTION

AN ANALYSIS of angle resolved u.v.-photoemission spectra is expected to give information about the electronic states at the solid surface, e.g. to determine the position of an adsorbate or the symmetry of a chemisorption state.

It is now clear that good agreement between experiments and calculations is achieved only if for the intial state the deformation of the atomic wave functions by the chemical binding [1] is taken into account as well as the final state [2, 23] includes the scattering by the atoms [3–7].

We study the effect of the polarization of the incident light on the angle resolved intensity distribution, including the case of unpolarized light. Particularly, the possibility of investigating the symmetry of the initial states is discussed. As an example we have calculated the emission from surface-localized states on the (001) surface of nickel which are introduced by the chemisorption of oxygen. Our conclusions are general and not restricted to this special system.

2. BASIC THEORETICAL CONSIDERATIONS

2.1. *Hamiltonian operator for the initial and final state*

The photoemission intensity (energy and angle resolved photocurrent) in the single particle approximation is given by a golden rule expression [8, 9]:

$$\frac{\mathrm{d}^2 j}{\mathrm{d}E_f \mathrm{d}\Omega} \sim \sqrt{E_f} \sum_k |\langle f|\mathbf{A}\nabla + \nabla\mathbf{A}|i_k\rangle|^2 \delta(E_f - E_{i_k} - \hbar\omega). \tag{1}$$

$\mathbf{A}$ is the vector potential. $\langle f|$ is the final state carrying the current into the solid angle Ω. $|i_k\rangle$ are the initial states of those electrons which contribute to the adsorbate-induced emission. They are eigenfunctions of an energy dependent Hamiltonian: The inelastic scattering of the final state is described by an imaginary part (of a few eV) of an optical potential equivalent to a mean free path of a few Å, while the initial state is a stationary solution in a real potential. Also the real part of the potential (including the exchange and correlation potential) is found to be a function of energy [10, 11].

Taking this into account the initial and final states are obtained as follows. The muffin tin concept is common to both Hamiltonians whereas the used models for the potential are different: For the initial chemisorption state we use potentials (and wave functions) from a self-consistent multiple-scattering calculation applied to a cluster of 6 atoms (SCF-$X\alpha$ [12]) whereas the final state is calculated by applying the multiple-scattering theory using potentials which give final states being in agreement with experimental LEED spectra.

2.2. *Barrier effect*

The surface barrier is assumed to lie outside the overlayer. According to the usual model for LEED the final state electron is only refracted but not reflected. Between barrier and overlayer we assume a (possibly infinitely thin) region of constant potential V_0. The refraction spreads the current contained in a cone $\mathrm{d}\Omega^{in} = \sin\theta^{in}\,\mathrm{d}\theta^{in}\,\mathrm{d}\phi$ in the region between overlayer and barrier into a cone $\mathrm{d}\Omega = \sin\theta\,\mathrm{d}\theta\,\mathrm{d}\phi$ in the vacuum. The conservation of the wave-vector component parallel to the surface yields

* This paper is a corrected version of *Solid State Commun.* 23, 789 (1977).

$$\sqrt{E_f}\sin\theta = \sqrt{E_f - V_0}\sin\theta^{in} \tag{2}$$

so that

$$\mathrm{d}\theta = \frac{\sqrt{E_f - V_0}\cos\theta^{in}}{\sqrt{E_f}\cos\theta}\,\mathrm{d}\theta^{in} \tag{3}$$

E_f and $(E_f - V_0)$ is the kinetic energy of the photoelectron in the vacuum and in the region between barrier and overlayer, respectively. The outer and inner intensities are therefore related from equations (3) and (2) by

$$\frac{\mathrm{d}^2 j}{\mathrm{d}E_f\mathrm{d}\Omega} = \frac{\mathrm{d}^2 j}{\mathrm{d}E_f\mathrm{d}\theta\sin\theta\,\mathrm{d}\phi} = \frac{\mathrm{d}^2 j}{\mathrm{d}E_f\mathrm{d}\Omega^{in}}\frac{E_f\cos\theta}{(E_f - V_0)\cos\theta^{in}}. \tag{4}$$

Even when the inner intensity is isotropic the outside intensity goes to zero with increasing polar angle. This reduction of intensity has often not been taken into account [2, 13, 14], but comparisons with experimental results have shown that it must be included in the calculated polar curves [4, 7].

2.3. *Polarization and reflection of the light*

We now show that the intensity of emission by excitation with unpolarized light is simply equal to the sum of the intensities excited by s- and by p-polarized light.

With the angle φ in a plane normal to the beam the vector potential of the incident light can be written as a superposition of s- and p-polarized contributions:

$$\mathbf{A}^0(\varphi) = \mathbf{A}_s^0\sin\varphi + \mathbf{A}_p^0\cos\varphi \tag{5}$$

where

$$|\mathbf{A}^0(\varphi)| = |\mathbf{A}_s^0| = |\mathbf{A}_p^0| = A^0 \tag{6}$$

states the randomness of the polarization. Because of linear response the vector potential including the refraction and reflection of the light can be expressed:

$$\mathbf{A}(\varphi) = \mathbf{A}_s\sin\varphi + \mathbf{A}_p\cos\varphi. \tag{7}$$

Since the scattering of light by the adsorbate layer is negligibly small, we neglect as a first approximation the influence of the adsorbate layer on the light and only take into account the refraction and reflection on the metal surface. The long-range variation of the vector potential $\mathbf{A}(\varphi)$ over the wavelength of the light is neglected in the matrix element as usual in the dipole approximation, but not the short-range variation of the normal component. Outside and inside near the surface this can be written with z normal to the surface:

$$A_z(z) = A_z^{\mathrm{out}}\,g(z). \tag{8}$$

In the macroscopic model of classical electrodynamics $g(z)$ is a step function which is unity outside and the dielectric function inside. It can be a more complicated function [15–17] without affecting our calculations and conclusions. The parallel components of the vector potentials are conserved across the boundary. For both sides near the metal surface we can express the s- and p-polarized vector potentials:

$$\mathbf{A}_s = (1 + r_s)\begin{pmatrix} -\sin\beta \\ \cos\beta \\ 0 \end{pmatrix} A^0 \tag{9a}$$

$$\mathbf{A}_p = \begin{pmatrix} (r_p - 1)\cos\beta\cos\alpha \\ (r_p - 1)\sin\beta\cos\alpha \\ (1 + r_p)\sin\alpha\, g(z) \end{pmatrix} A^0 \tag{9b}$$

β is the azimuth angle of the incident light beam and α is the polar angle, r_s and r_p are the complex reflectivities for s- and p-polarized light. To get the intensity of emission by unpolarized light we have to sum over all random polarization angles φ. This yields vanishing interference terms between s- and p-polarized excitation.

$$\frac{\mathrm{d}^2 j_{\mathrm{unpol}}}{\mathrm{d}E_f\mathrm{d}\Omega} \sim |\langle f|\mathbf{A}_p\nabla + \nabla\mathbf{A}_p|i\rangle|^2 + |\langle f|\mathbf{A}_s\nabla + \nabla\mathbf{A}_s|i\rangle|^2 \sim \frac{\mathrm{d}^2 j_s}{\mathrm{d}E_f\mathrm{d}\Omega} + \frac{\mathrm{d}^2 j_p}{\mathrm{d}E_f\mathrm{d}\Omega} \tag{10}$$

Combining (9) and (10) yields

$$\frac{\mathrm{d}^2 j_s}{\mathrm{d}E_f\mathrm{d}\Omega} \sim (2A^0)^2\left|1 + r_s\right|^2\left|\left\langle f\left|\frac{\partial}{\partial y}\right|i\right\rangle\cos\beta - \left\langle f\left|\frac{\partial}{\partial x}\right|i\right\rangle\sin\beta\right|^2 \tag{11}$$

$$\frac{\mathrm{d}^2 j_p}{\mathrm{d}E_f\mathrm{d}\Omega} \sim (2A^0)^2\left|\left\langle f\left|\frac{\partial}{\partial x}\right|i\right\rangle(r_p - 1)\cos\beta\cos\alpha + \left\langle f\left|\frac{\partial}{\partial y}\right|i\right\rangle(r_p - 1)\sin\beta\cos\alpha + \frac{1}{2}\left\langle f\left|\frac{\partial g(z)}{\partial z} + 2g(z)\frac{\partial}{\partial z}\right|i\right\rangle(1 + r_p)\sin\alpha\right|^2. \tag{12}$$

The matrix elements in equations (11) and (12) are independent of the direction of the light beam. The formulae (11), (12) are the basis of our calculations.

2.4. *Alternative forms of the matrix element*

For evaluating the matrix elements in (11) and (12) we use the velocity form $\langle f|\partial/\partial x|i\rangle$ and also the acceleration form $\langle f|[(\partial/\partial x)V]|i\rangle$. These are proportional within the approximation that the difference between the final state and the initial state potentials is spatially constant [18]. The differences between the different forms of the optical transition matrix elements are discussed by Holland [14] within the approximation

of a spherical energy-independent potential and a constant vector potential. It is shown that the acceleration form puts more weight on contributions to the matrix element from the region near the nucleus while the velocity form should be preferred if the wave functions are most accurate at intermediate distances.

3. PARAMETERS AND CALCULATION SCHEMES

The structures of $c(2 \times 2)$ and $p(2 \times 2)$O on Ni has been analysed successfully by recent dynamical LEED intensity analysis [19, 20]: The oxygen atom sits 0.9 Å above the first Ni layer and occupies the four-fold symmetric hollow of the Ni (001) surface.

Our *initial states* are described by LCAOs centered on the oxygen and on the four nearest neighbour nickel atoms. They are fitted to the results of a chemisorption cluster calculation (SCF-$X\alpha$) [12]. Arguments for a justification of localized initial states are the relatively large distances of the adsorbed atoms and essentially no dispersion of the energy levels, as seen in angle resolved photoemission for both superstructures [21]. Group theory predicts two levels for our case: With z normal to the surface there should be one level of symmetry a_1 which is derived from the O $2p_z$ state and a doubly degenerate level of symmetry e derived from O $2(p_x, p_y)$. The nomenclature of the states refers to the irreducible representation of the C_{4V} point group.

For calculating the *final state* the time reversal symmetry is used [8, 9, 36]: The time reversed final state is an incoming plane wave which is scattered by the crystal including the overlayer so that a certain combination of spherical waves is built up around the adsorbate and its neighbours. To determine this combination of spherical waves we calculate the time reversed final state using the multiple scattering theory (LEED) [22]. The electron–electron interaction is approximated by a constant complex optical potential. The inner potential (muffin tin zero) and the imaginary part of the optical potential are taken from bulk nickel [11] and extended into the overlayer region:

$$V_0 = -13.5\,\text{eV} \qquad V_i = -2.5\,\text{eV}.$$

The wave function between the layers is represented by 50 plane waves. For describing the scattering by atoms of the substrate and the overlayer 5 phase shifts are used. Nickel phase shifts are taken from a Wakoh-potential and oxygen phase shifts from a Mattheiss-potential [11, 34]. Final state calculations are checked by reproducing LEED spectra (Fig. 1) which show good agreement with experimental results [24] especially at the energies of He II photoelectrons, i.e. at about 30 eV.

We have used two different ways for evaluating the matrix elements of equations (11) and (12). In the first method the transition matrix element is evaluated in

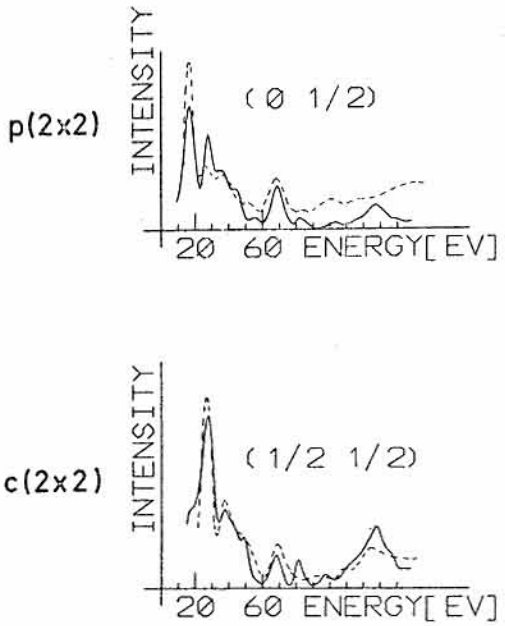

Fig. 1. Calculated LEED spectra of the first adsorbate-induced spots for the two different superstructures of O on Ni (001). Dashed curves are experimental results [24].

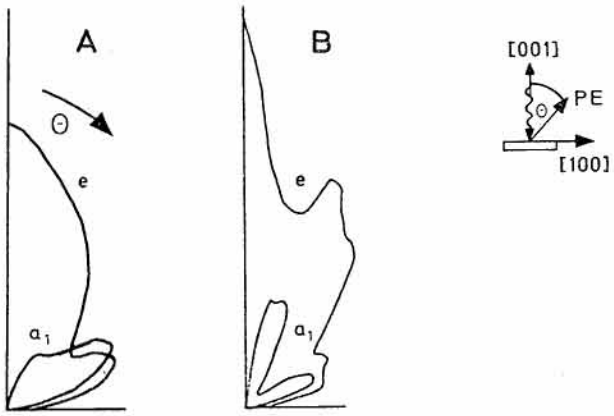

Fig. 2. Calculated polar angle dependence from adsorbate levels of symmetry a_1 (O $2p_z$-derived) and e (O $2(p_x, p_y)$-derived), O $p(2 \times 2)$ on (001) Ni. Excitation with normal incidence of unpolarized light. (A) initial states LCAO; final state: LEED pseudo wave; final state energy: 11 eV ($\hbar\omega = 21.2$ eV). (B) initial states: LCAO; final state: LEED pseudo wave; final state energy: 30.6 eV ($\hbar\omega = 40.8$ eV).

k-space. $\mathbf{k}_\parallel$ is conserved modulo a reciprocal lattice vector parallel to the surface and the k_z integration is done numerically. We use as the final state the LEED pseudo-wave function, which is the correct wave function between the muffin tins but fails near the atom centers. Therefore we have used the velocity form of the matrix element (see Section 2.4).

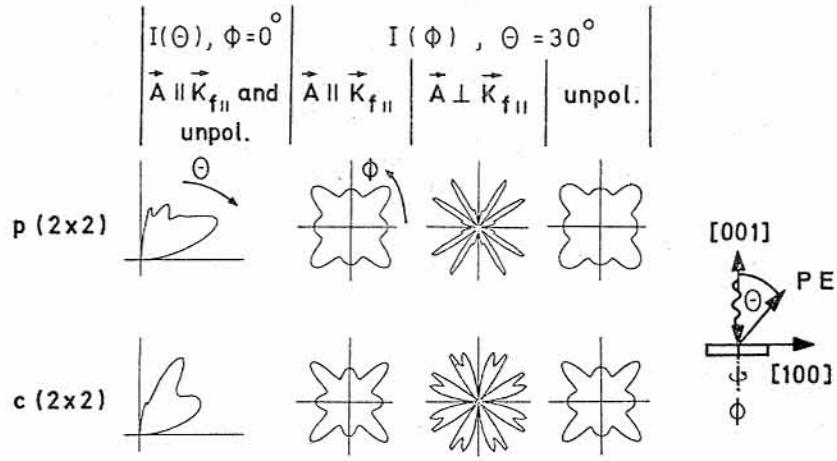

Fig. 3. Angular distribution from O $2p_z$ state of O on Ni (001) into a multiple scattered final state for two different adsorbate superstructures. Excitation with He II (final state energy: 30.6 eV), for different polarizations with the vector potential A parallel to the surface. $k_{f\parallel}$ is the projection of the wave vector of the photoelectron on the surface. Curves are normalized to maximum.

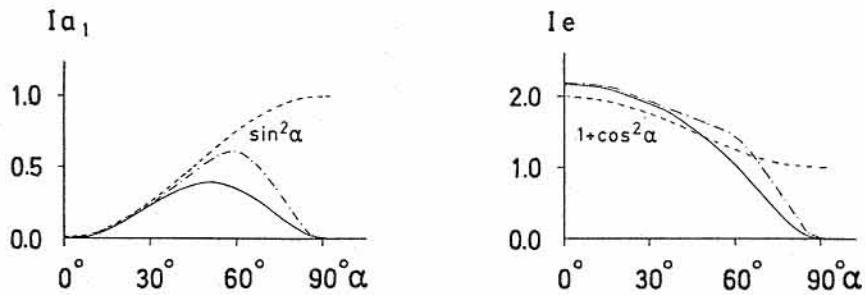

Fig. 4. Emission normal to the surface from a system of C_{4V} symmetry, i.e. from adsorbate levels of symmetry a_1 (p_z-derived) and e ((p_x, p_y)-derived), as a function of the polar angle of an unpolarized light beam. Full curve: He I light ($\hbar\omega = 21.2$ eV), dot–dashed curves: He II light ($\hbar\omega = 40.8$ eV), dashed curves: reflection of the light neglected.

The other method is not based on the use of the pseudo-wave function. The matrix element is evaluated in angular momentum representation, using the acceleration form within the approximation of a spatially constant difference between final state and initial state potentials. This is the convenient form due to the muffin tin potential because only the regions inside the muffin tin spheres contribute to the matrix elements.

4. ANGULAR DISTRIBUTIONS OF PHOTOELECTRONS (FIXED LIGHT SOURCE)

In Fig. 2 we show the influence of the photon energy on calculated angular distribution curves for excitation with unpolarized light of normal incidence. The fine structure of the curves decreases at lower photon energy. The *general* structure is independent of the photon energy whereas for different initial states it is characteristically different. The general structure near normal emission can be understood by a selection rule (see Section 5). Normal to the surface there is vanishing emission from the a_1-level but non-zero intensity from the e-level [13, 25], whereas at high polar angles ($\theta \gtrsim 70°$) the behaviour of the curves is determined by the refraction effect (see Section 2.2).

These curves of Fig 2 are calculated by evaluating the optical transition matrix elements in k-space, using the LEED pseudo-wave function for the final state.

In Fig. 3 we show curves for excitation with polarized normal incident light for two different superstructures. The initial state is only the atomic O $2p_z$ state which is the dominant atomic orbital of the a_1-level [12, 26], the final state is the correct multiply scattered wave. The method used here is the angular momentum representation and the acceleration form but curves of the same structure were obtained by the other method.

It should be noted that the third column of Fig. 3 is essentially determined by a selection rule [13, 27]: for a level which has the same symmetry as the crystal (this is the a_1-state but not the e-states) there is no emission into the mirror planes of the crystal when the vector potential **A** lies perpendicular to the mirror plane. Such azimuthal curves, therefore, show directly the number of mirror planes and, for example, it should be possible to distinguish between the two-fold (bridge) position and a four-fold position of the adsorbate or to distinguish between a four-fold site of bond coordination two or four [28, 29]. This selection rule has the consequence that the emission into directions in a mirror plane from an a_1-state is identical for s-polarized light if the incident light beam lies in a plane perpendicular to the mirror plane and for normal incidence of unpolarized light (Fig. 3, first column). The absolute intensities in the third column of Fig. 3 are only 4–10% of those in column 2. Therefore the characteristic structure of column 3 is not seen with unpolarized light in column 4.

Similar selection rules are also valid for the emission from the e-states but have no such dramatic effect on the angular distribution because of the degeneracy: The emission into a mirror plane of the crystal only comes from the states which have the same symmetry as the operator $(\nabla\mathbf{A} + \mathbf{A}\nabla)$ relative to that mirror plane. Therefore the degenerate e-states can be observed separately by polarized excitation (**A** in the surface, parallel and perpendicular to the mirror plane).

5. EMISSION DEPENDENCE ON THE POLAR ANGLE OF AN UNPOLARIZED LIGHT BEAM

We will derive two simple formulae describing the intensity at normal emission as a function of the polar angle of the light beam, considering as an example the C_{4V} symmetry of an adsorbate on the (001) surface of Ni. These formulae have been used to classify peaks in experimental curves according to the symmetry of the initial states [7].

Mahan [9] has suggested in his surface photo-effect model that the emission dependence on the polar angle α of light should be determined by the surface barrier and therefore it should be proportional to $\sin^2(\alpha)$. Feibelman [18] has modified this function by taking into account, as we do, the reflection of the light. In contrast to these authors we assume the surface barrier to refract the final-state electron but not to determine the angular dependence of the emission essentially. The comparison with experimental data indicates that this treatment is sufficiently realistic [7, 30].

We will evaluate equations (10), (11) and (12) only using symmetry properties (selection rules) of the system. Similar arguments have been used before for the interpretation of angular resolved photoemission spectra by polarized excitation [27, 31–33].

It should be noted that at normal emission the final state is of a_1-symmetry. The product of the initial state times the operator $(\nabla\mathbf{A} + \mathbf{A}\nabla)$ must also be of symmetry a_1 for a non-vanishing matrix element. Therefore only an initial a_1-state with polarization normal to the surface or an initial state of the irreducible representation e with the polarization vector parallel to the surface can be observed at normal emission [27].

The axes x and y are assumed to lie in mirror planes of the C_{4V} symmetry. We find at once selection rules for the transition from the a_1-state into the normal emission final state:

$$\left\langle f\left|\frac{\partial}{\partial x}\right|a_1\right\rangle = \left\langle f\left|\frac{\partial}{\partial y}\right|a_1\right\rangle = 0 \tag{13}$$

because $|a_1\rangle$ and $|f\rangle$ are both symmetric with respect to the mirror planes containing the x and the y axes, whereas the operator $\partial/\partial x$ or $\partial/\partial y$ respectively is antisymmetric. The emission dependence from a_1-level is, therefore, from equations (10)–(12):

$$\left.\frac{\mathrm{d}^2 j(\alpha)_{\mathrm{unpol}}}{\mathrm{d}E_f \mathrm{d}\Omega}\right|_{\substack{\theta=0 \\ E_f = E_{a_1} + \hbar\omega}} \sim |1 + r_p|^2 \sin^2\alpha. \tag{14}$$

The two e-states are labeled as e_x (p_x-derived) and e_y (p_y-derived):

$$\left\langle f\left|\frac{\partial g(z)}{\partial z} + 2g(z)\frac{\partial}{\partial z}\right|e_x\right\rangle = \left\langle f\left|\frac{\partial g(z)}{\partial z} + 2g(z)\frac{\partial}{\partial z}\right|e_y\right\rangle = 0 \tag{15}$$

$$\left\langle f\left|\frac{\partial}{\partial x}\right|e_y\right\rangle = \left\langle f\left|\frac{\partial}{\partial y}\right|e_x\right\rangle = 0 \tag{16}$$

$$\left\langle f\left|\frac{\partial}{\partial x}\right|e_x\right\rangle = \left\langle f\left|\frac{\partial}{\partial y}\right|e_y\right\rangle . \tag{17}$$

The contributions from the degenerate e-states add incoherently to give:

$$\left.\frac{\mathrm{d}^2 j(\alpha)_{\mathrm{unpol}}}{\mathrm{d}E_f \mathrm{d}\Omega}\right|_{\substack{\theta=0 \\ E_f = E_e + \hbar\omega}} \sim |1 - r_p|^2 \cos^2\alpha + |1 + r_s|^2 . \tag{18}$$

Both formulae (14) and (18) are independent from the azimuth angle of the light beam. They are evaluated using Fresnel formulae for r_s and r_p [7] and the optical data for Ni at the frequencies of the He I and He II lines [35]:

$$\epsilon_{\mathrm{Ni}}(21.2\,\mathrm{eV}) = 0.48 + i0.85$$

$$\epsilon_{\mathrm{Ni}}(40.8\,\mathrm{eV}) = 0.78 + i0.27.$$

The resulting curves are shown in Fig. 4 and compared to the intensity dependence resulting from formulae (14) and (18) if reflection of the light is neglected.

Such curves including reflection have been observed

in the emission from oxygen and carbon monoxide on nickel (001) [7, 30, 37].

6. CONCLUSIONS

There are special geometric arrangements of the directions of light incidence, emission direction and symmetry planes, for which an interpretation of angular-resolved photoemission intensity curves is possible by means of selection rules, even for unpolarized light.

The general structure of the polar angle distribution of photoelectrons by excitation with normal incidence of unpolarized light (or *s*-polarized light of arbitrary incidence) is characteristically determined by the initial state symmetry. It is understood at small polar angles by selection rules and at high polar angles by refraction at the surface barrier. Only initial states of symmetry *e* contribute to the normal emission. The calculated examples give large intensity normal to the surface, caused by the non-plane-wave character of the final state. At high polar angles ($\theta \gtrsim 70°$) in general the intensity decreases to zero (roughly proportional to $\cos\theta$).

Also the normal emission as a function of the direction of an unpolarized light beam is discussed. It is found that it depends only on the initial state symmetry and therefore it can be used for its identification.

Further the use of polarized light (**A** in the surface, normal to $\mathbf{k}_{f\parallel}$) makes it possible to identify the initial state symmetry. In the case of an initial state with a *s*- or p_z-like symmetry the azimuthal dependence directly shows the number of mirror planes of the initial state, because there is no emission into the mirror planes.

Acknowledgements – The authors thank Dr. N. Rösch for supplying the SCF-$X\alpha$ data. They thank Prof. K. Molière for interest and support, and Dr. K. Jacobi for valuable discussions. The continuous help of L. Schulz is gratefully acknowledged. The work was supported in part by the Deutsche Forschungsgemeinschaft.

REFERENCES

1. GADZUK J.W., *Phys. Rev.* **B10**, 5030 (1974); **12**, 5608 (1975); *Surf. Sci.* **53**, 132 (1975).
2. LIEBSCH A., *Phys. Rev. Lett.* **32**, 1203 (1974); *Phys. Rev.* **B13**, 544 (1976).
3. DAVENPORT J.W., *Phys. Rev. Lett.* **36**, 945 (1976).
4. SMITH R.J., ANDERSON J. & LAPEYRE G., *Phys. Rev. Lett.* **37**, 1081 (1976).
5. APAI G., WEHNER P.S., WILLIAMS R.S., STÖHR J. & SHIRLEY D.A., *Phys. Rev. Lett.* **37**, 1497 (1976).
6. LIEBSCH A., *Solid State Commun.* **19**, 1193 (1976).
7. JACOBI K., SCHEFFLER M., KAMBE K. & FORSTMANN F., *Solid State Commun.* **22**, 17 (1977).
8. FEIBELMAN P.J. & EASTMAN D.E., *Phys. Rev.* **B10**, 4932 (1974).
9. MAHAN G.D., *Phys. Rev.* **B2**, 4334 (1970).
10. LUNDQUIST B.I., *Phys. Status Solidi* **32**, 273 (1969).
11. DEMUTH J.E., MARCUS P.M. & JEPSEN D.W., *Phys. Rev.* **B11**, 1460 (1975).
12. RÖSCH N. & MENZEL D., *Chem. Phys.* **13**, 243 (1976); RÖSCH N. (private communication).
13. SCHEFFLER M., KAMBE K. & FORSTMANN F., *Proc. Int. Symp. on Photoemission, Noordwijk, The Netherlands*, 13–16 Sept. 1976 (Edited by WILLIS R.F., FEUERBACHER B., FITTON B. & BACKX C.), p. 227. ESA, ESTEC, Noordwijk, Netherlands.
14. HOLLAND B.W. (to be published).
15. KLIEWER K., *Phys. Rev.* **B14**, 1412 (1976).
16. FEIBELMAN P.J., *Phys. Rev.* **B12**, 1319, 4282 (1975).
17. FORSTMANN F. & STENSCHKE H., *Phys. Rev. Lett.* **38**, 1365 (1977).
18. FEIBELMAN P.J., *Surf. Sci.* **46**, 558 (1974).
19. DEMUTH J.E., JEPSEN D. & MARCUS P.M., *Phys. Rev. Lett.* **31**. 540 (1973).
20. VAN HOVE M. & TONG S.Y., *J. Vac. Sci. Techn.* **12**, 230 (1975).
21. JACOBI K. (private communication).
22. PENDRY J.B., *Low Energy Electron Diffraction.* Academic Press, London (1974).
23. TONG S.Y. & VAN HOVE M., *Solid State Commun.* **19**, 543 (1976).
24. DEMUTH J.E. & RHODIN T.N., *Surf. Sci.* **45**, 249 (1974).

25. LIEBSCH A., *Phys. Rev. Lett.* **38**, 248 (1977).
26. BATRA I.P. & ROBAUX O., *Surf. Sci.* **49**, 653 (1975).
27. HERMANSON J., *Solid State Commun.* **22**, 9 (1977).
28. HAGSTRUM H.D. & BECKER G.E., *J. Vac. Sci. Techn.* **14**, 369 (1977).
29. FISHER G.B., *Surf. Sci.* **62**, 31 (1977).
30. HORN K., BRADSHAW A.M. & JACOBI K. (to be published).
31. GOBELI G.W., ALLEN F.G. & KANE E.O., *Phys. Rev. Lett.* **12**, 94 (1964).
32. DIETZ E., BECKER H. & GERHARDT U., *Phys. Rev. Lett.* **36**, 1397 (1976).
33. LAPEYRE G.J., SMITH R.J. & ANDERSON J., *J. Vac. Sci. Techn.* **14**, 384 (1977).
34. PENDRY J.B. (private communication).
35. WEHENKEL C. & GAUTHE B., *Phys. Status Solidi (b)* **64**, 515 (1974).
36. ADAWI I., *Phys. Rev.* **134**, A788 (1964).
37. WEEKS S.P. & PLUMMER E.W., *Solid State Commun.* **21**, 695 (1977).